4878 *Macromolecules* **2009**, *42*, 4878–4886
DOI: 10.1021/ma900479y

Macromolecules
ARTICLE

Properties of Dendrimers with Flexible Spacer-Chains: A Monte Carlo Study

J. S. Kłos*,†,§ and J.-U. Sommer†,‡

†*Leibniz Institute of Polymer Research Dresden e.V., 01069 Dresden, Germany,* ‡*Institute for Theoretical Physics, Dresden University of Technology, 01069 Dresden, Germany, and* §*Faculty of Physics, A. Mickiewicz University, Umultowska 85, 61-614 Poznań, Poland*

Received March 6, 2009; Revised Manuscript Received April 21, 2009

ABSTRACT: We study the properties of starburst dendrimers with flexible spacers in good solvent using Monte Carlo simulations based on the bond fluctuation model by systematic variation of dendrimers' generation number G and spacer length S. Our simulations support the dense-core picture of dendrimers due to a substantial decrease of monomer densities with the radial distance from the dendrimers' center of mass. The interior of dendrimers is penetrated by the terminal groups due to finite values of the end-group densities in that area indicating backfolding of the terminal groups toward the molecules' interior. The mean instantaneous shape of dendrimers changes monotonously from oblate to spherical as the increase in their molecular weight N is caused by an increase in G, while for fixed G it is hardly affected by variations of S. Using a mean-field model for the dendrimer extension reveals spacers as nearly unperturbed linear chains in good solvent and the dendrimer's conformation is a result of rearrangement of spacer chains up to a limiting generation of about $G = 9$. In particular, the radius of gyration follows the predicted scaling behavior of $R_g/S^{\nu} \sim (N/S)^{1/5}G^{2/5}$. Upon appropriate rescaling of length scales, extension measures, monomer distributions, and shape factors display spacer-length scaling. As a result dendrimers in good solvent display universal properties with respect to the length of spacers up to a rather high number of generations.

I. Introduction

Starburst dendrimers are macromolecules with a hierarchical, treelike architecture that is also named the Caley tree.[1,2] The most widespread methods of making such highly branched molecules by chemical synthesis are referred to as divergent and convergent, respectively. In the former approach, starting from the core, new branched units of monomers are attached to the outermost ones so as to form the next generation. In the latter, first the branched arms, i.e., dendrons, are prepared, and they are finally attached to the multifunctional core.[3,4] Apart from their purely scientific value dendrimers have become useful in industry, biomedicine, pharmacy, and materials engineering. Actually, lithographic materials, nanoscale catalysts, drug delivery systems, rheology modifiers, bioadhesives, and MRI contrast agents are examples of their potential applications.[5−8]

Theoretical studies carried out on dendrimers make use of such analytical techniques as mean-field models, self-consistent methods, renormalization group techniques and Flory-type approaches. On- and off-lattice simulations, on the other hand, involve the kinetic self-avoiding-walk, Brownian/molecular dynamics and Monte Carlo algorithms. Among others these methods enable an insight into such crucial issues concerning dendrimers as scaling of their size with the number of monomers, shape anisotropy, internal fractal structure, structure factor, radial monomer/terminal-group densities, and phase properties.[9−34] Furthermore, apart from static properties, simulations allow an inspection of dynamical behavior of the macromolecules. Actually, dendrimer translational self-diffusion, the size and shape fluctuations, rotational mobility, and elastic motions have been considered numerically as well.[19,35,36] Experimental studies, in turn, employ for example photochemical and spectroscopic probe methods, mass spectrometry, translational diffusion and viscometry.[37−39] Furthermore, transmission electron (TEM) and atomic force microscopy (AFM) as well as small-angle neutron (SANS) and X-ray (SAXS) scattering methods are used to elucidate the shape and internal structure of dendrimers.[27,40−46]

In this paper, we perform lattice Monte Carlo simulations based on the bond fluctuation model (BFM) of dendrimers. To the best of our knowledge, this is one of the first applications of the BFM to such highly branched molecules, [47] which however proves efficient and allows a systematic inspection of dendrimers in a wide range of generations G and spacer lenghts S. In our studies we focus on static properties of dendrimers and address the issues of their instantaneous shape observed for various molecular weights N, scaling of the radius of gyration and the center-to-end-bead distance with N as well as spacial distribution of monomers and terminal groups. In particular, we show that depending on G and S there is a rich variety of monomer/terminal-group density profiles that support the dense-core picture of dendrimers andthe phenomenon of the end-group's backfolding. Our findings indicate that dendrimers of low generations are oblate shaped, whereas spherical shape is gradually recovered for high-generation molecules. Finally, the obtained computational data provide a confirmation of the most general form of the scaling prediction for the radius of gyration in which both G and S are independent parameters, and additionally enable us to propose another scaling formula for the center-to-end-bead distance.

The rest of the paper is organized as follows: In sections II and III we outline the model, the simulation method and the scaling prediction for the dendrimers' extension, respectively. The results of our simulations are presented and discussed in section IV. Finally, our conclusions and remarks are given in section V.

*Corresponding author.

 Published on Web 05/21/2009

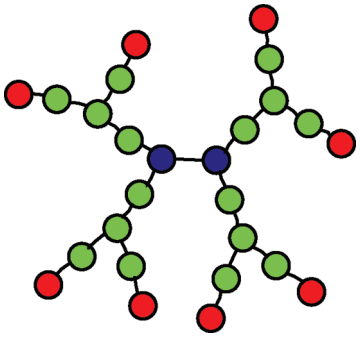

Figure 1. 2*D* sketch of dendrimer architecture for the generation number $G = 2$ and spacer length $S = 2$. The red circles represent the terminal groups, the blue ones the core.

II. Model and Simulations

In the present work we carry out Monte Carlo simulations using the bond fluctuation method on a cubic lattice.[48,49] We benefit from the advantages of this algorithm, which by definition secures the excluded volume condition and prevents the bonds from crossing. It is suited for simulations of linear chains as well as molecules with a highly branched architecture of their skeleton. In particular, for the latter molecules, the algorithm enables proper moves both for monomers constituting linear parts of the molecules and for the branches.

The systems of interest contain single dendrimers with movable centers on a cubic lattice. In the simulations a cubic box of the size $L^3 = 800 \times 800 \times 800u^3$ (where u is the length unit) is used with periodic boundary conditions in all three dimensions. The molecules are treelike collections of beads connected by the BFM lattice bonds so as to form the macromolecular skeleton (for a 2*D* schematic representation of dendrimers see Figure 1). Before simulation runs, dendrimers with generation G, spacer length S and branching functionality $f = 3$ are generated by a divergent growth process in the ascending order of the internal generation number $0 \le g \le G$ starting from the core ($g = 0$) of two bonded monomers. Thus, the molecules consist of

$$N = 2 + 4S(2^G - 1) \tag{1}$$

monomers,

$$N_t = 2^{G+1} \tag{2}$$

of which are the terminal groups. In the paper we inspect model dendrimers of generations ranging between $G = 1$ and $G = 10$ with the upper bound of molecular weight $N \approx 8000$ (see Table 1). Furthermore, due to recent progress in chemical synthesis both short and long spacers with length given by $S = 2^k$, $k = 0, ..., 6$ are considered.[47] In our studies, depending on G and S the systems were equilibrated for a maximum of 10^7 MCS (Monte Carlo steps; one MCS consists of N random selections of monomers to be moved in a randomly chosen, one of the six directions by a single lattice unit), whereas averages were calculated for 10^3-10^5 equilibrium configurations stored every 10^4th MCS. Since merely the excluded volume interactions between monomers and bond constraints are taken into account the obtained results are athermal.

III. Mean-Field Model and Spacer-Scaling

The extension of a dendrimer, R, will be largely controlled by excluded volume effects because of the exponential growth of the number of monomers at higher generations. Nevertheless, at low numbers of generations we might assume that individual threads of the dendrimer (linear branches reaching from the center to the end-monomers) follow single chain excluded volume statistics, i.e. $R \sim (SG)^\nu$, where ν denotes the Flory exponent with the best estimates of $\nu \simeq 0.588$. Using Flory-type free energy balance arguments the value of $\nu = {}^3/_5$ is appropriate. When the number of generations is increased the crowding of spacers will lead to deviations from single chain statistics as has been considered in previous work.[9,10] Let us apply a simple mean-field argument for the free energy of a thread (energy units of kT, length unit is the bond length), see refs 10, 30, and 50:

Table 1. The Visited Systems

$G\backslash S$	1	2	4	8	16	32	64
1	6	10	18	34	66	130	258
2	14	26	50	98	194	386	770
3	30	58	114	226	450	898	1794
4	62	122	242	482	962	1922	3842
5	126	250	498	994	1986	3970	7938
6	254	506	1010	2018	4034	8066	-
7	510	1018	2034	4066	8130	-	-
8	1022	2042	4082	8162	-	-	-
9	2046	4090	8178	-	-	-	-
10	4094	8186	-	-	-	-	-

$$F = \frac{R^2}{SG} + v_0 \frac{SGN}{R^3} \tag{3}$$

Here, v_0 denotes the strength of excluded volume interaction. For simplicity, we suppress constant prefactors in the simple argument. Here, the first contribution corresponds to stretching of the thread using the ideal extension ${R_0}^2 \sim SG$. All excluded volume effects are considered in the second term. The second term denotes the average pair interaction of the thread with all the other monomers. Minimization of eq 3 leads to[30,50]

$$R \sim (SG)^{2/5} N^{1/5} \tag{4}$$

This law is expected to hold merely in a scaling regime below a maximium number of generations, G_{max}, such that the average monomer volume density is rather low.[30] We note, this model applies to a dense core picture, where the monomers are rather homogeneously distributed within the dendrimers' volume, see section IV.IV.

In order to better understand eq 4, it can be rewritten as follows:

$$R/S^\nu \sim (nG^2)^{1/5} \tag{5}$$

where we have used $\nu = {}^3/_5$ corresponding to the mean-field model and we have introduced the number of spacer chains $n = N/S$. The right-hand side is independent of the spacer-length since the number of spacer chains is only defined by the functionality and the number of generations. For our simulations we have $N/S \simeq 4 \times 2^G$, see eq 1. Thus, the free spacer-chain extension sets the characteristic length scale. This result can be also obtained by considering the spacer chains as blobs which interact with an effective excluded volume interaction of the order of kT. As a consequence, the mean-field model predicts the extension of dendrimers to be the result of rearrangement of spacer chains instead of stretching the spacer chains themselves.

As mentioned above, mean-field or scaling arguments can only be valid up to a maximum generation where the spacer chains are densely packed. In this state the dendrimer defines a c^*-network of spacer chains. Given that at the maximum generation the radius of the dendrimer scales as GS^ν, we obtain for maximum packing the relation: $4 \times 2^G \approx G^3$. This limit is reached for $G_{max} \simeq 10$.

We note that the mean-field argument predicts a larger extension of the dendrimer as compared to the c^*-dendrimer

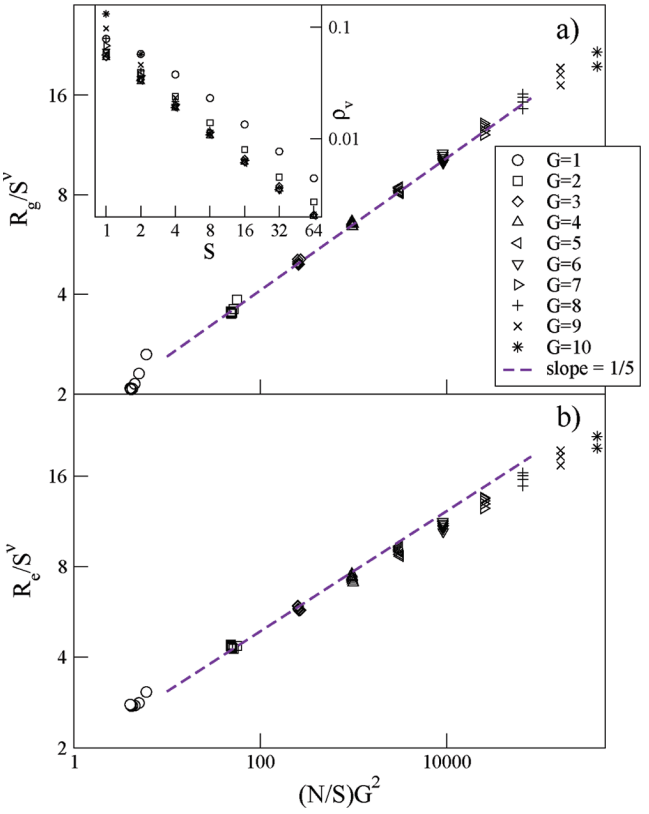

Figure 2. (a) Scaling plot of R_g/S^ν and (b) R_e/S^ν versus $(N/S)G^2$ for all the visited systems. The dashed line indicates the slope of $^1/_5$ as predicted in the mean-field model. The inset shows the monomer volume density ρ_v versus S.

which is obtained by densely packing the unperturbed spacer chains for $G < G_{max}$:

$$R/S^\nu \sim \left(\frac{N}{S}\right)^{1/3} \tag{6}$$

In fact, mean-field argument implies a larger scale of unscreened excluded volume and a more open structure. Note that our estimate for G_{max} follows by eqs 5 and 6.

The simple arguments presented in this section involve a couple of assumptions which can only be justified by experiments or simulations. However, they provide a background for the discussion of various results. In particular the spacer-scaling is a strong prediction which can be tested in various observables. We start the presentation of our simulation results with an analysis of the characteristic extensions of the dendrimer. Then, we turn to the investigation of the density profiles and the shape of the dendrimers.

IV. Results

A. Size of the Dendrimer. We can consider at least two measures for the extension of the dendrimer: The radius of gyration, R_g, and the distance between the end-monomers and the center of mass, R_e. In Figure 2, we plot both variables using the scaling prediction according to eq 5. Obviously, the scaling is obeyed reasonably for both observables up to the 7th generation. With respect to the predicted exponent of $^1/_5$, we observe good agreement for the radius of gyration of the dendrimers but some deviation for R_e. As presented in the inset of Figure 2, the monomer volume fraction $\rho_v = 3N/4\pi R_g^3$ is low to moderate and is the highest for the smallest spacer length. Except for $G = 10$, $S = 1$ the density is less than 0.1, which is below the concentrated state in the

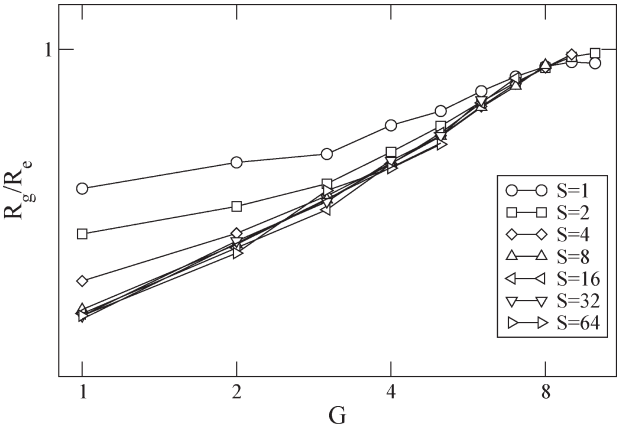

Figure 3. Ratio of the characteristic length scales R_g/R_e vs the number of generations.

BFM-model. This concurs with our observation about the scaling regime in the sense of eq 4.

In order to analyze the difference in the behavior of the radius of gyration and R_e we present the ratio of both quantities R_g/R_e as a function of the number of generations in Figure 3. We can observe a monotonous increase of the characterstic ratio with respect to the number of generations which falls into a master curve for larger length of spacers. This indicates a slightly different explicit generation dependence of R_e. Let us assume a more general dependence of R_e with respect to the three quantities according to

$$R_e \sim G^\alpha S^\gamma N^\beta \tag{7}$$

In the upper panel of Figure 4 in the double logarithmic scale R_e versus N for specified values of G is shown. As it is seen, for each G the data perfectly collapse on a number of parallel lines. Fitting them with $\gamma = 2/5$ gives in each case $\beta_G \approx {}^1/_5$, though some tendency of β_G to increase with G is present (see Table 2). Thus, we confirm the spacer-length scaling ($\beta = {}^1/_5$ and $\gamma = {}^2/_5$) for R_e in the form

$$R_e/S^\nu \sim G^\alpha \left(\frac{N}{S}\right)^{1/5} \tag{8}$$

We have found the best fit to our data using $\alpha = 0.3$ (instead of $\alpha = 0.4$ according to the mean-field argument). In Figure 4b, we show $R_e/G^{0.3}$ as a function of N for fixed spacer length S. Again for each S the data points almost perfectly crumple into parallel lines with the exponent $\beta_S \approx {}^1/_5$ (see Table 3). Finally, in Figure 4c) $R_e/G^{0.3}S^{2/5}$ is plotted versus N for all the points available and their collapse on the master line is seen. As required, the value of the exponent β calculated using all the points as a single data set is again close to $^1/_5$ ($\beta = 0.207$). Note, that like the scaling of R_g, some deviation from eq 7 is again observed for the same dendrimer ($G = 10$, $S = 1$) with the highest equilibrium monomer volume density ρ_v. Moreover, from eq 7 and eq 4 it follows that for given $G \geq 2$, S and N the expression

$$Z = R_g R_e^{-1} G^{-1/10} \tag{9}$$

should be constant. A closer inspection displays some systematic deviations from this prediction although in a narrow range of a few percent which indicates that a modified exponent α might oversimplify the G-dependence of the characterstic ratio R_g/R_e.

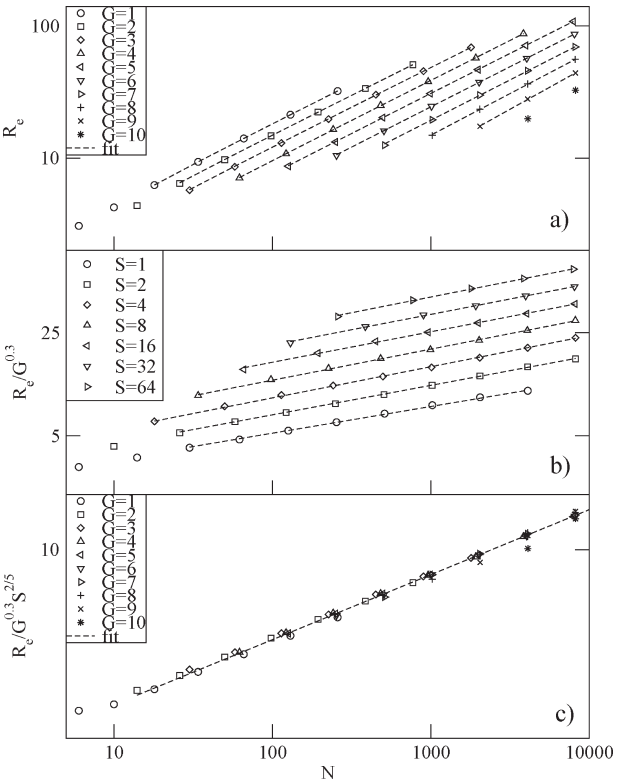

Figure 4. (a) R_e versus N for fixed generations G and variable spacer length S. (b) $R_e/G^{0.3}$ versus N for fixed S and variable G. (c) $R_g/G^{0.3}S^{2/5}$ versus N for all the visited systems. The dashed lines show the fits to the data.

Table 2. Fitting Parameter β_G for Fixed Generation Number G and Variable Spacer Length S

	$G = 1$	$G = 2$	$G = 3$	$G = 4$	$G = 5$	$G = 6$	$G = 7$	$G = 8$	$G = 9$
β_G	0.198	0.198	0.199	0.204	0.205	0.207	0.210	0.229	0.265

Table 3. Fitting Parameter β_S for Fixed Spacer Length S and Variable Generation Number G

	$S = 1$	$S = 2$	$S = 4$	$S = 8$	$S = 16$	$S = 32$	$S = 64$
β_S	0.180	0.199	0.211	0.210	0.207	0.208	0.212

The strong conclusion about spacer scaling can be proved directly by calculating the radius of gyration of spacers of different lengths in dendrimers of different generations. The result is displayed in Figure 5. The extension of the spacers does not depend on the number of generations in the given range and displays excluded volume scaling.

To conclude this section we found that spacer-length scaling is obeyed and can be observed in both measures of the dendrimer's size where the free extension of the spacer sets the relevant length scale, and $R_e/S^{3/5}$ and $R_g/S^{3/5}$ depend only on the branching parameters. However, the characteristic ratio, R_g/R_e, varies systematically with the number of generations.

B. Density Profiles. We now turn to the properties of the spatial distribution of the monomers and terminal groups with respect to their distance from the molecules' center of mass. It is worth emphasizing at this point that especially the former is open to dispute and its unique picture is still missing. The earliest analysis based on the self-consistent field theory using a force balance argument for the branching points led to the dense-shell model with the monomer density

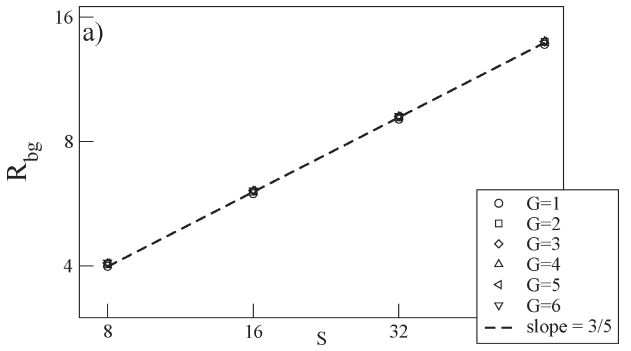

Figure 5. Averaged radius of gyration of spacers as a function of their length. The dashed line indicates the Flory exponent.

profile increasing monotonously outward from the center and the terminal groups located on the dendrimers' periphery.[9] However, later calculations without any coinstraint imposed on the terminal groups and computer simulations using a kinetic growth algorithm brought about a different picture of dendrimers referred to as the dense-core model, in which the monomer density is maximal at the center and decreases to zero *strictly* monotonously.[10,11,17,42−44,46] Most of the Monte Carlo and molecular dynamics simulation studies confirm the dense-core model, but unlike the analytical results they predict for high generation dendrimers profiles with a local minimum near the center followed by a broad plateau in the interior and a peripherial zone.[12,15,20,22,24−26,29,30,51] Furthermore, a number of numerical studies demonstrate a similar behavior of the monomer density throughout the volume occupied by dendrimers, except for the vicinity of the center where a hole in the profiles is detected.[16,27] On the other hand, there is no such controversy about the location of the terminal groups. In spite of some differences in the details of the actual shape of the end-group profiles, analytical calculations as well as simulations report on significant backfolding of the end-groups toward the dendrimers' domain.[10−12,15,16,19,22,25,27,29−31] In particular, it has been demonstrated that the profiles possess either a single maximum or a plateau for dendrimers of low and high generations, respectively.[22,42,43,45,46] A number of studies have also brought about multimodal shapes of end-group densities.[15,16,31] It should also be stressed that at least to some extent the results obtained with theoretical studies on dendrimer's mass and terminal-group distribution are consistent with observations provided by small-angle neutron and X-ray scattering experiments.[27,42,43,45,46]

In Figure 6, we display the monomer density ρ_m defined as the fraction of occupied lattice sites within a shell of thickness u (lattice unit) versus the rescaled radial distance r/R_g from the center for fixed values of the spacer length, S, as a function of the number of monomers N caused by variations of G. In particular, for molecules with the shortest spacers $S = 1$ and $S = 2$, it shows how the monotonously decaying profiles turn into ones with a plateau as the generation G is increased. The crossover appears for $G \approx 5$ above which both the width and the actual value of the plateau grow monotonously with G. Thus, in this respect, our results are consistent with a number of previous simulation studies where a similar qualitative change in the shape of ρ_m with increasing G was observed,[15,22,25,26,29,30] and this supports the dense-core picture of dendrimers.

In order to study the effect of spacer length for a given generation of a dendrimer, we consider a spacer chain as a flexible polymer chain in good solvent. In the unperturbed

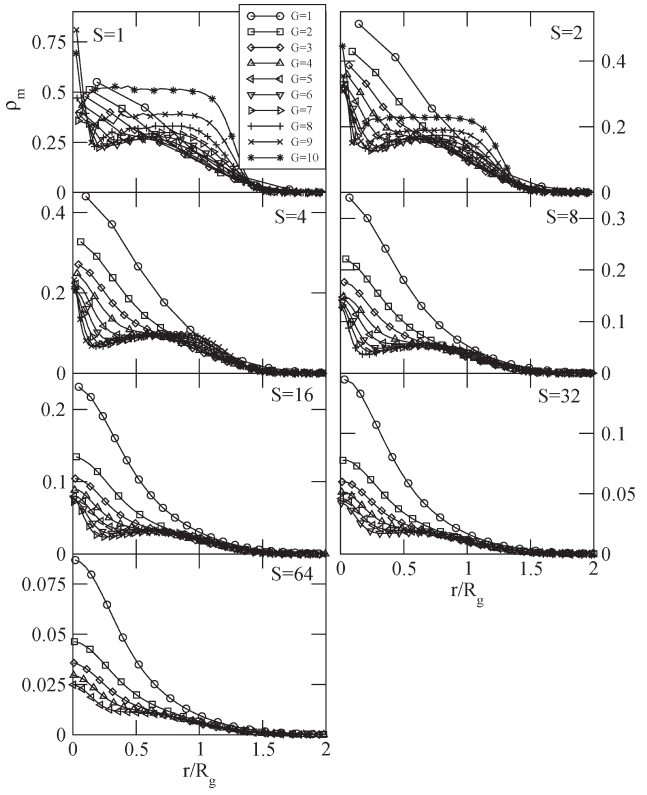

Figure 6. Radial monomer density ρ_m versus the rescaled distance from the dendrimers' center of mass r/R_g for specified spacer length S and variable generation G.

state the typical extension of the spacer chain is given by $R_S \sim S^{\nu}$ with a self-density of $(S/R_S^3) \sim S^{1-3\nu}$. The mean-field argument as well as the results for the dendrimers extension indicate that the spacer chains display free excluded volume behavior up to a limiting value of the number of generations. Therefore, we have plotted in Figure 7 the rescaled monomer density $\rho_m/S^{1-3\nu}$ versus the rescaled radial distance r/S^{ν} with respect to the center for fixed values of G. The density follows the scaling prediction nicely up to the generation number of $G = 8$. However, for higher generations only small spacer lengths are realized and the validity of the excluded volume scaling is much restricted. Deviations from scaling can be observed for small distances and smaller length of spacers. Moreover, for the lowest generations $G \leq 4$ the radial density decays to zero with r/S^{ν} strictly monotonously, whereas for molecules of higher generations it behaves differently. In the latter case near the center a sharp reduction in $\rho_m S^{3\nu-1}$ down to a local minimum occurs and is subsequently followed by a relatively broad local maximum. Therefore, the monomers penetrating the latter area constitute the actual dendrimers' domain. Note that for the highest generations inspected ($G \geq 8$) $\rho_m S^{3\nu-1}$ practically reaches a plateau and that for $G = 10$, $S = 1$ this plateau corresponds to a dense melt of monomers with $\rho_m \approx 0.5$.

Next, we analyze the spatial distribution of the terminal groups. In Figure 8, the rescaled end-bead radial density $\rho_e S^{3\nu}$ is plotted versus r/S^{ν} for specified values of G and variable S. It is clearly seen that the terminal monomers evidently penetrate the whole dendrimers' domain, which provides an evidence for their backfolding. Note that for $G \leq 4$ the profiles are bell shaped, whereas for higher generations they again broaden and flatten or even become bimodal (see Figure 9). Obviously this qualitative change in the end-profiles' shape corresponds to that discussed above for monomer density ρ_m.

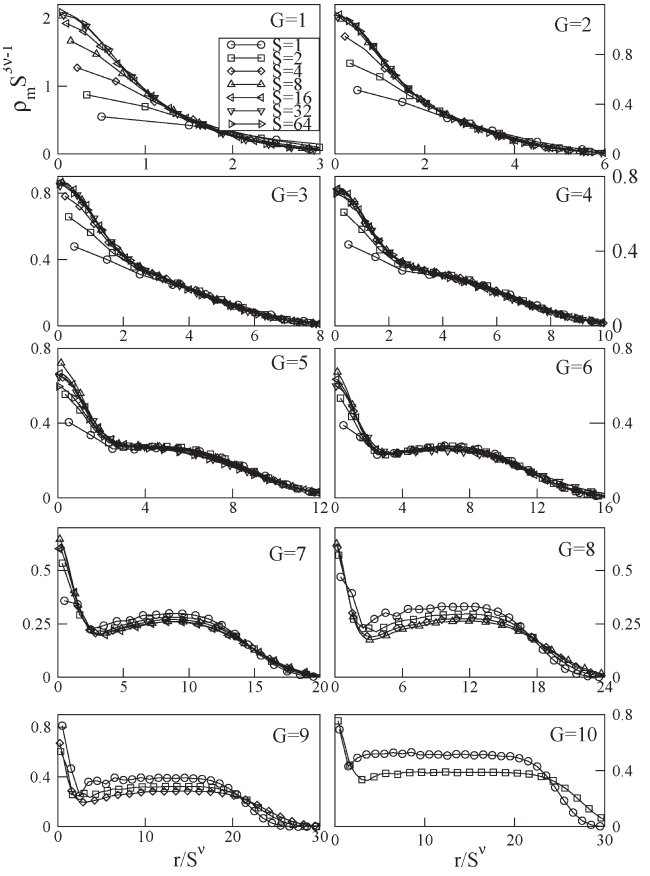

Figure 7. Rescaled radial monomer density $\rho_m S^{3\nu-1}$ versus the rescaled distance from the dendrimers' center of mass r/S^{ν} for specified generation G and variable spacer length S.

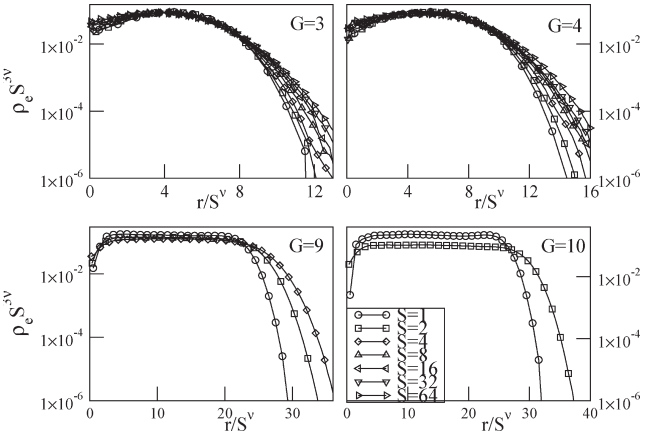

Figure 8. Rescaled radial density of the terminal groups $\rho_e S^{3\nu}$ versus the rescaled distance from the dendrimers' center of mass r/S^{ν} for specified generation G and variable spacer length S. The vertical axis is in the logarithmic scale.

In Figures 10 and 11, we display the distribution of branching monomers of the internal generations (including the terminal groups) $0 \leq g \leq G$ denoted by $\rho_{b,g}$.[26,29] For the core monomers $\rho_{b,0}$ is characterized by a very high peak in the center and a sharp decrease around it. For $g > 0$ and dendrimers of lower G the density is bell shaped with a single maximum in the domain (see Figure 10). With increasing g the profiles broaden and the position of their maximum shifts outward from the center which indicates that the branching points become more and more delocalized in space. In other words they penetrate all the interior including

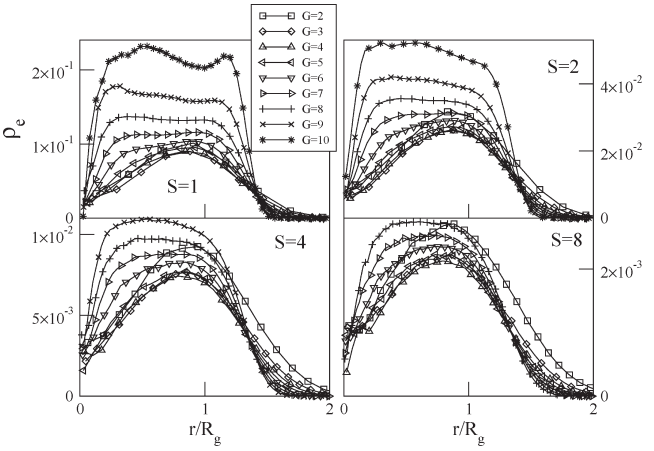

Figure 9. Radial density of the terminal groups ρ_e versus the rescaled distance from the dendrimers' center of mass r/R_g for specified spacer length S and variable generation G.

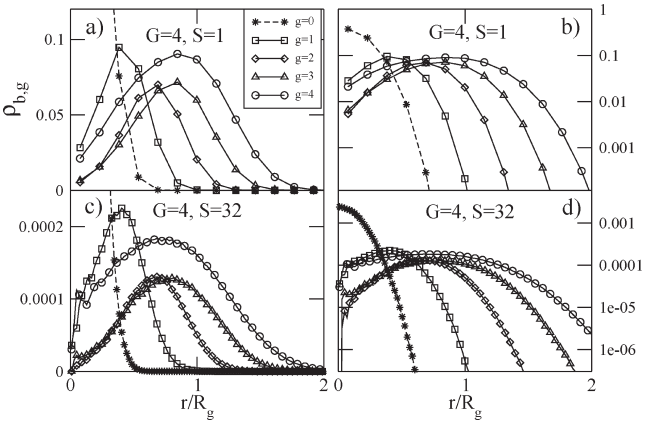

Figure 10. Radial density $\rho_{e,g}$ of the branching monomers within the dendrimer of generation $G = 4$ versus r/R_g for $S = 1$ (a), $S = 32$ (c). Plots b and d show the same as a and c, respectively, with the vertical axis in the logarithmic scale. The dashed curves show $\rho_{e,0}$.

the neighborhood of the dendrimers' center. On the other hand, in the extreme of dendrimers of high G the branching points of the first few internal generations with $g > 0$ are well localized since their distributions are narrow and peak-shaped (see Figure 11). In particular, they do not explore the shell surrounding the center. Above a certain value of g, however, the branching points again reveal a tendency to penetrate most of the dendrimers' domain. This tendency strengthens with g and is reflected in the corresponding profiles that tremendously broaden and flaten. Actually, for the dendrimer shown in Figure 11a) the branching points belonging to the internal generations with $g > 7$ are already distributed all over the molecules' interior with the corresponding density $\rho_{b,g}$ nearly constant, and decresing sharply near the center. As it is seen in Figure 11c) this kind of delocalization of the branching points occurs even for ones of smaller g when the spacer length S is larger. Note that throughout the domain the density of the delocalized monomers is considerably greater than of the localized ones due to the larger number of the former. Therefore, in the particular case of $S = 1$, in which the densities $\rho_{b,g}$ sum up to the overal ρ_m the above observations suggest that for dendrimers of high G the sharp decrease near the center and the plateau within the interior seen in ρ_m are due to the contributions from the core monomers and the outermost branching ones, respectively. Similarly, the monotonously decaying density ρ_m detected for low generation dendrimers with $S = 1$

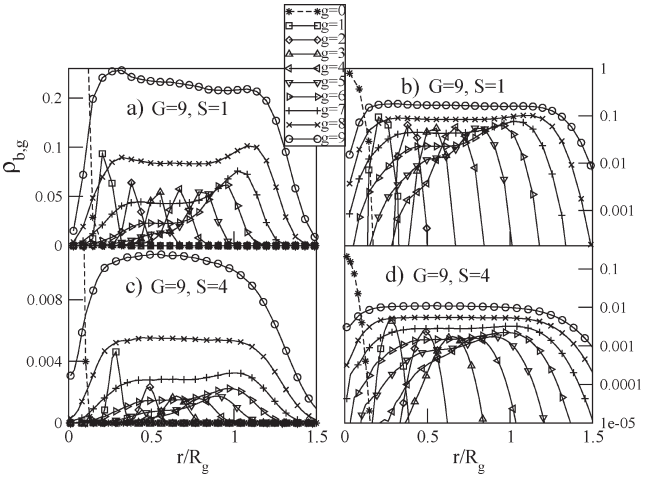

Figure 11. Radial density $\rho_{e,g}$ of the branching monomers within the dendrimer of generation $G = 9$ versus r/R_g for $S = 1$(a), $S = 4$ (c). Plots b and d show the same as plots a and c, respectively, with the vertical axis in the logarithmic scale. The dashed curves show $\rho_{e,0}$.

corresponds to the sharp density of the core beads and a lack of plateau in the other $\rho_{b,g}$.

Summarizing this section, we conclude that distribution both of the monomers and of the terminal groups display spacer-length scaling over a wide range. All simulation results confirm the dense-core picture in which ρ_m is the highest in some neighborhood of the molecules' center, and depending on G, either reaches a plateau or continues to decay in a monotonous manner as the domain is approached. For higher generations the branching points belonging to the first few internal generations are localized inside a shell, whereas the outer branching points (including the terminal groups) are distributed throughout the molecules. A few snapshots of dendrimers of various generations and spacers are displayed in Figure 12.

C. Shape of Dendrimers. The instantaneous shape of a polymer molecule usually breaks spherical symmetry. A linear chain, for instance, displays a prolate ellipsoidal shape.[52,53] Note, that it is important to distinguish between the shape observed with and without orientational averaging because only the latter can become aspherical in an otherwise isotropic environment. This, for instance, can play a role in such phenomenon as viscous flow or diffusion of dendrimers, which in turn, may be crucial to the practical use of them. The question of dendrimers' shape has been directly dealt with by transmission electron microscopy (TEM) measurements of individual dendrimer molecules of poly (amidoamine) (PAMAM), and from the stained images it has been concluded that to a first approximation dendrimers of generations between $G = 7$ and $G = 10$ are spherical in shape, though a more detailed inspection suggests that they are rather polyhedronlike objects.[40] Moreover, some simulation studies complement the experiment and indicate asymmetric shapes of dendrimers of low generations G and nearly spherical shapes of molecules of higher G.[16,19,25,28]

The instantaneous shape of polymers can be analyzed quantitatively by means of the radius of gyration tensor[16,52,54]

$$R_{\mu\nu} = (1/N)[\sum_{i}^{N}(r_{\mu i} - r_{cm,\mu})(r_{\nu i} - r_{cm,\nu})], \qquad \mu, \nu = x, y, z \quad (10)$$

where $r_{\mu i}$ and $r_{cm,\mu}$ are the coordinates of the ith monomer and of the center of mass of the molecule in the laboratory frame of

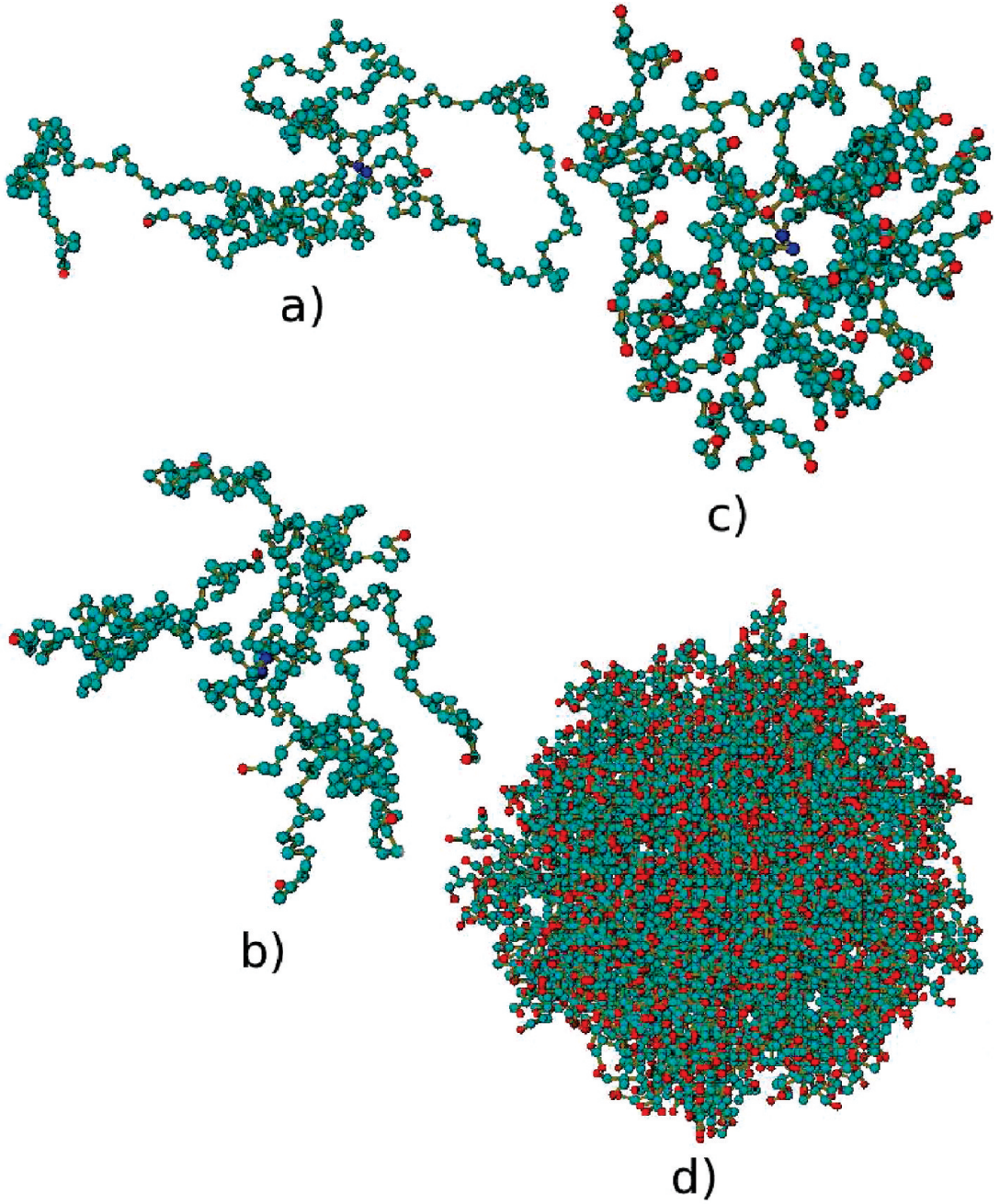

Figure 12. Snapshots of dendrimers of $G = 1, S = 64$ (a), $G = 2, S = 32$ (b), $G = 5, S = 4$ (c), $G = 10, S = 2$ (d). The red spheres represent the terminal monomers and the blue ones the core.

reference, respectively. From the definition 10 it follows that $R_{\mu\nu}$ is real and symmetric and therefore it can be diagonalized by a linear transformation to the principial axis system in which the eigenvalues I_x, I_y, I_z of $R_{\mu\nu}$ are real and positive. These eigenvalues correspond with semiaxes of $3D$ ellipsoides that within this kind of approach represent polymers. More specifically, the two invariants I_1, I_2 of $R_{\mu\nu}$ out of the three

$$I_1 = \mathrm{Tr}(R_{\mu\nu}) = I_x + I_y + I_z = {R_g}^2, \quad I_2 = I_xI_y + I_xI_z + I_yI_z, I_3 = I_xI_yI_z \tag{11}$$

where R_g stands for the radius of gyration, are used to define the so-called relative shape anisotropy[16,52,54]

$$a = 1 - 3I_2/{I_1}^2 \tag{12}$$

which takes values between 0 and 1. In particular, $a = 0$, $a = {}^1/_4$, and $a = 1$ for spherical, oblate and extremely elongated ellipsoides, respectively. Furthermore, an insight into the anisotropy of the polymeric ellipsoides can also be gained more directly by the so-called aspect ratios defined as ($I_z \le I_y \le I_x$)

$$a_{xy} = I_x/I_y, \quad a_{xz} = I_x/I_z \tag{13}$$

Note that the calculation of the ensemble averages of the above quantities requires that $R_{\mu\nu}$ is diagonalized in every stored equilibrium conformation.

In Figure 13a, we show the average relative shape anisotropy a as a function of the number of spacer chains N/S. Generally, we observe a tendency of this quantity to drop from higher values of $a = 0.25$ to nearly isotropic behavior $a = 0.05$ when increasing the molecular weight by variation

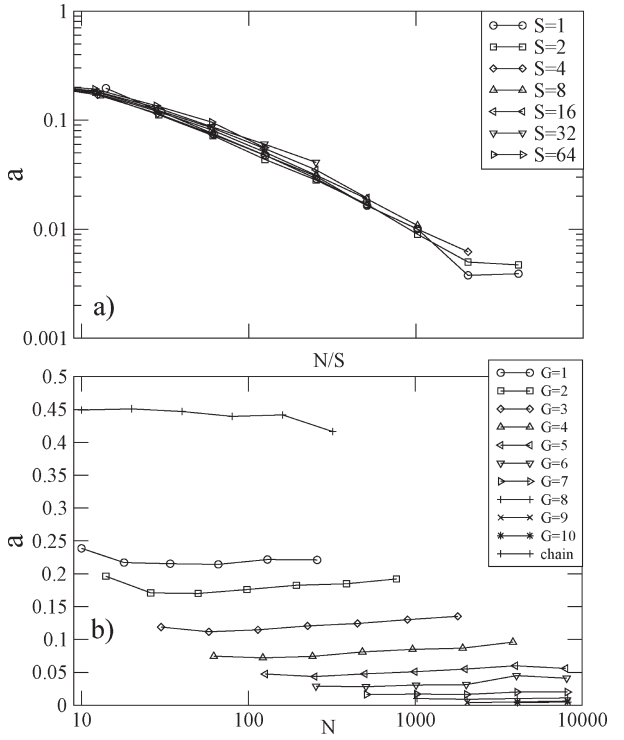

Figure 13. (a) Average relative shape anisotropy a versus the molecular weight per spacer N/S for specified spacer length S. (b) Average relative shape anisotropy for specified generation G. For the sake of comparison the bottom picture also shows a calculated for a number of linear chains.

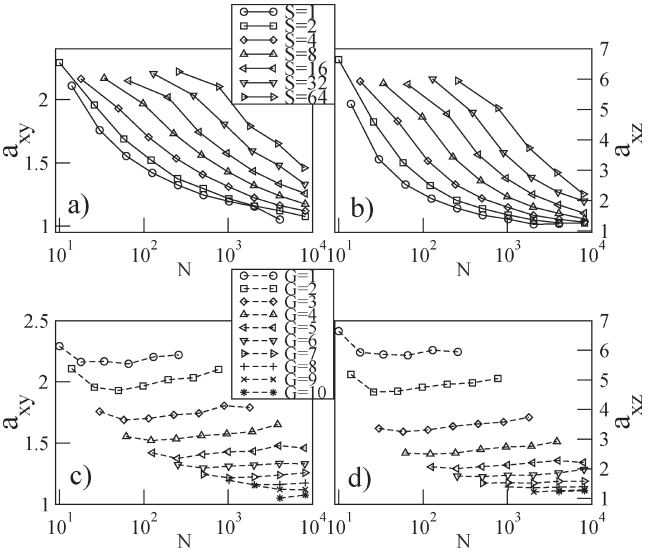

Figure 14. (a) Aspect ratios a_{xy}, (b) a_{xz} for specified spacer length S and variable generations G. (c) Aspect ratios a_{xy}, (d) a_{xz} for specified generations G and variable S.

of G, and to be rather independent of the spacer length S. In accordance with a number of previous studies[19,25] the observed change in a is smooth and monotonous and does not reveal a local minimum.[16] The dependence of the average anisotropy on S when G is specified is minor in particular for spacers with $S > 2$, and the actual value of a is determined by G itself (Figure 13b). Thus, spacer-length scaling, though not perfect, can be observed in Figure 13a). In Figure 14, we have displayed the aspect ratios a_{xy} and a_{xz}; see eq 13. In the limit of low generations the actual values of the aspect ratios support the picture of oblate shaped objects

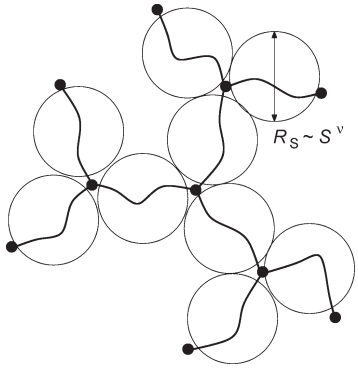

Figure 15. Spacer chains of a dendrimer in a good solvent can be considered as nearly unperturbed blobs. The dendrimer's conformation results from rearrangements of spacer chains to minimize excluded volume interactions.

because $2 < a_{xy} < 2.5$ and $6 < a_{xz} < 7$. Thus, we can conclude that dendrimers of low generations are represented by oblate-shaped ellipsoides that become nearly spherical with increasing generation number G. We note that spacer-length scaling can be applied to the aspect ratios as for the averaged anisotropy but it is not shown in the plots.

We conclude that it is rather the generation number G and not the spacer length S that controls the instantaneous shape of dendrimers, which is generally oblate tending to isotropic at higher generations.

V. Conclusions

We have used the bond fluctuation method to study dendrimers in a wide range of generations and spacer lengths under athermal solvent conditions. On the grounds of a variety of density profiles, we have confirmed the dense-core picture of dendrimers. In the case of dendrimers of low generations, their mass density decays strictly monotonously with the distance from the molecule's center, while a sharp decrease in the density near the center and a broad plateau in the interior occur for higher generation molecules. Our simulations have also provided evidence of dispersion of the branching points as well as the terminal groups throughout the molecules. For dendrimers of high generations this backfolding is best pronounced for the terminal groups and the outer branches, whereas the inner ones are strongly localized. With respect to the instantanous shape of dendrimers our findings indicate that there is a smooth transition from oblate to spherical shapes in going from low to high generations.

Reformulation of the mean-field model for the dentrimer size reveals spacer sequences as nearly unperturbed linear chains in good solvent. The length scales of various observables such as the extension, density profiles and shape factors can be expressed in terms of unperturbed spacer-chain size, and all properties of dendrimers with flexible spacers depend essentially on the number of generations only. This picture has been confirmed by our simulation results. Monomer and terminal-group distributions collapse over a wide range when spacer-length scaling is applied. Also the shape factors display scaling and thus shape anisotropy is hardly sensitive to variations of the spacer. The radius of gyration displays scaling with the predicted slope of $^1/_5$ with respect to the molecular mass of the dendrimer. We found that the characteristic ratio between the radius of gyration and the mean distance of the terminal groups from the center of mass varies systematically with the number of generations. This effect might be attributed to the increasing backfolding with increasing number of generations as observed in the distribution of terminal groups. As a result of our study, we find that many properties of

the dendrimer, up to the limiting generation of about 9 for 3-functional branching points, are independent of spacer length upon appropriate rescaling of length scales. Thus, we arrive at a picture sketched in Figure 15 where the spacers can be considered as blobs which are nearly unperturbed, and the conformation of the dendrimer is basically the result of rearrangement of spacer chains to reduce excluded volume interactions. At a limiting generation the dendrimer forms a c^*-network of spacer blobs. Higher generations lead to penetration of spacer chains up to a close-packed state (melt) at the highest possible generation.

Acknowledgment. We gratefully acknowledge financial support from the Deutsche Forschungsgemeinschaft (DFG).

References and Notes

(1) Tomalia, D. A.; Baker, H.; Dewald, J. R.; Hall, M.; Kallos, G.; Martin, S.; Roeck, J.; Ryder, J.; Smith, P. *Polym. J.* **1985**, *17*, 117.
(2) Buhleier, E. W.; Wehner, W.; Vogtle, F. *Synthesis* **1978**, *1978*, 155.
(3) Hodge, P. *Nature* **1993**, *362*, 18.
(4) Hawker, C. J.; Frechét, J. M. J. *J. Am. Chem. Soc.* **1990**, *112*, 7638.
(5) Lee, C.; MacKey, J. A.; Frechéet, J. M. J.; Szoka, F. C. *Nat. Biotechnol.* **2005**, *23*, 1517.
(6) Majoros, I.; Baker, J. R. *Dendrimer-Based Nanomedicine*, 1st ed.; Pan Stanford Publishing Pte. Ltd.: Singapore, **2008**.
(7) Svenson, S.; Tomalia, D. A. *Adv. Drug Delivery Rev.* **2005**, *57*, 2106.
(8) Klajnert, B.; Bryszewska, M. *Acta Biochim. Pol.* **2001**, *48*, 199.
(9) Gennes, P. G. D.; Hervet, H. *J. Phys., Lett.* **1983**, *44*, 251.
(10) Boris, D. ; Rubinstein, M. *Macromolecules* **1996**, *29*, 7251.
(11) Zook, T. Z.; Picket, G. T. *Phys. Rev. Lett.* **2003**, *90*, 015502.
(12) Timoshenko, E. G.; Kuznetsov, Y. A.; Connolly, R. *J. Chem. Phys.* **2002**, *117*, 9050.
(13) Lyulin, S. V.; Evers, L.; van der Schoot, P.; Darinskii, A.; Lyulin, A. V.; Michels, M. A. J. *Macromolecules* **2004**, *37*, 3049.
(14) Gotze, I. O.; Archer, A. J.; Likos, C. N. *J. Chem. Phys.* **2006**, *124*, 084901.
(15) Gotze, I. O.; Likos, C. N. *Macromolecules* **2003**, *36*, 8189.
(16) Maiti, P. K.; Çağin, T.; Wang, G.; Goddard, W., III. *Macromolecules* **2004**, *37*, 6236.
(17) Lescanec, R. L.; Muthukumar, M. *Macromolecules* **1990**, *23*, 2280.
(18) Lescanec, R. L.; Muthukumar, M. *Macromolecules* **1991**, *24*, 4892.
(19) Karatasos, K.; Adolf, D. B.; Davies, G. R. *J. Chem. Phys.* **2001**, *115*, 5310.
(20) Karatasos, K. *Macromolecules* **2005**, *38*, 4472.
(21) Suek, N. W.; Lamm, M. H. *Macromolecules* **2006**, *39*, 4247 .
(22) Giupponi, G.; Buzza, D. M. A. *Macromolecules* **2002**, *35*, 9799.
(23) Wallace, E. J.; Buzza, D. M. A.; Read, D. J. *Macromolecules* **2001**, *34*, 7140.
(24) Lyulin, A. V.; Davies, G. R.; Adolf, D. B. *Macromolecules* **2000**, *33*, 6899.
(25) Mansfield, M. L.; Klushin, L. I., *Macromolecules* **1993**, *26*, 4262.
(26) Mansfield, M. L.; Jeong, M. *Macromolecules* **2002**, *35*, 9794.
(27) Rathgeber, S.; Pakula, T.; Urban, V. *J. Chem. Phys.* **2004**, *121*, 3840.
(28) Naylor, A. M.; Goddard, W. A.; Keiffer, G. E.; Tomalia, D. A. *J. Am. Chem. Soc.* **1989**, *111*, 2339.
(29) Murat, M.; Grest, S. G. *Macromolecules* **1996**, *29*, 1278.
(30) Chen, Z. Y.; Cui, S. M. *Macromolecules* **1996**, *29*, 7943.
(31) Zacharopoulos, N.; Economou, I. G.; *Macromolecules* **2002**, *35*, 1814.
(32) Rissanou, A. N.; Economou, I. G.; Panagiotopoulos, A. Z., *Macromolecules* **2006**, *39*, 6298.
(33) Zhou, T.; Chen, B. *Macromolecules* **2006**, *39*, 6686.
(34) Biswas, P.; Cherayil, B. J. *J. Chem. Phys.* **1994**, *100*, 3201.
(35) Lyulin, A. V.; Davies, G. R.; Adolf, D. B. *Macromolecules* **2000**, *33*, 3294.
(36) Lyulin, S. V.; Darinskii, A. A.; Lyulin, A. V.; Michels, M. A. *Macromolecules* **2004**, *37*, 4676.
(37) Jockusch, S.; Ramirez, J.; Sanghvi, K.; Nociti, R.; Turro, N. J.; Tomalia, D. A. *Macromolecules* **1999**, *32*, 4419.
(38) Weener, J. W.; van Dongen, J. L. J.; Meijer, E. W. *J. Am. Chem. Soc.* **1999**, *121*, 10346.
(39) Pavlov, G. M.; Korneeva, E. V.; Meijer, E. W. *Colloid Polym. Sci.* **2002**, *280*, 416.
(40) Jackson, C. L.; Chanzy, H. D.; Booy, F. P.; Drake, B. J.; Tomalia, D. A.; Bauer, B. J.; Amis, E. J. *Macromolecules* **1998**, *31*, 6259.
(41) Li, J.; Piehler, L. T.; Quin, D.; Baker, J. R.; Tomalia, D. A. *Langmuir* **2000**, *16*, 5613.
(42) Potschke, D.; Ballauff, M.; Lindner, P.; Fischer, M.; Vogtle, F. *Macromolecules* **1999**, *32*, 4079.
(43) Potschke, D.; Ballauff, M.; Lindner, P.; Fischer, M.; Vogtle, F. *Macromol. Chem. Phys.* **2000**, *201*, 330.
(44) Likos, C. N.; Schmidt, M.; Lowen, H.; Ballauff, M.; Potschke, D.; Lindner, P. *Macromolecules* **2001**, *34*, 2914.
(45) Rosenfeldt, S.; Dingenouts, N.; Ballauff, M.; Werner, N.; Vogtle, F.; Lindner, P. *Macromolecules* **2002**, *35*, 8098.
(46) Prosa, T. J.; Bauer, B. J.; Amis, E. J. *Macromolecules* **2001**, *34*, 4897.
(47) Rangou, S.; Theodorakis, P. E.; Gergidis, L. N.; Avgeropoulos, A.; Efthymiopoulos, P.; Smyrnaios, D.; Kosmas, M.; Vlahos, C.; Giannopoulos, T. *Polymer* **2007**, *48*, 652 .
(48) Carmesin, I.; Kremer, K. *Macromolecules* **1988**, *21*, 2819.
(49) Trautenberg, H. L.; Holzl, T.; Goritz, D. *Comput. Theor. Polym. Sci.* **1996**, *6*, 135.
(50) Sheng, Y. J.; Jiang, S.; Tsao, H. K. *Macromolecules* **2002**, *35*, 7865.
(51) Ballauff, M.; Likos, C. N., *Angew. Chem., Int. Ed.* **2004**, *43*, 2998.
(52) Theodoru, D. N.; Suter, U. *Macromolecules* **1985**, *18*, 1206.
(53) Doi, M.; Edwards, S. F. *The Theory of Polymer Dynamics*, 2nd ed.; Oxford University Press Inc.: Oxford, U.K., **1998**.
(54) Rudnick, J.; Gaspari, G. *J. Phys. A: Math. Gen.* **1986**, *19*, L191.